QFT Design of a PI Controller with Dynamic Pressure Feedback for Positioning a Pneumatic Actuator

Mark Karpenko and Nariman Sepehri

Abstract— **Quantitative feedback theory (QFT) is applied towards the design of a simple and effective position controller for a typical low-cost industrial pneumatic actuator with a 5-port three-way control valve, that is subject to disturbing forces. A simple fixed-gain proportional-integral control law with dynamic pressure feedback is synthesized to guarantee the satisfaction of a priori specified closed-loop performance requirements, including robust stability, tracking performance and disturbance attenuation, despite the presence of nonlinearities and parametric uncertainty in the pneumatic functions. A novel outer-inner design approach is proposed to avoid the synthesis of an unnecessarily complex outer loop controller. The merits of the inner loop feedback are examined from the perspective of system responses to step changes in the reference position and step changes in the disturbing force. Simulation results show clearly that the inner loop feedback improves the closed-loop disturbance response by eliminating oscillation and reducing the overshoot. The main contribution of this paper is the presentation of a systematic approach to the design of position controllers for pneumatic servos with dynamic pressure feedback, within the framework of QFT.**

I. Introduction

A number of different approaches to controller design for highly nonlinear pneumatic positioning systems have been explored in the literature. To name a few, Liu and Bobrow [1] investigated proportional-derivative (PD) as well as optimal linear quadratic Gaussian (LQG) controls. Sliding mode control [2], Neural network control [3], Fuzzy logic [4], as well as Neuro-Fuzzy control [4] have also been tried for various servopneumatic positioning systems. Robust control techniques such as modern H_∞ and classical quantitative feedback theory (QFT) have received comparatively little attention in the fluid power literature, especially with regard to pneumatic systems. However, H_∞ and QFT control of pneumatic actuators have been recently examined in [5] and [6], respectively. From the perspective of controller design for pneumatic servos the QFT design methodology is attractive since it highly transparent [7] and has the capacity, at the design stage, to account for the effects of the nonlinear pneumatic functions and plant parametric uncertainty. This paper further explores the application of QFT towards effective position control of pneumatic actuators, particularly in the presence of disturbing forces. The goal is to apply the QFT methodology towards synthesis of a simple and practical position controller for a typical industrial pneumatic actuator controlled by a low-cost 5-port three-way valve.

First, proportional-integral (PI) compensation only in a typical two degree-of-freedom control structure is examined. It is shown that a PI control law alone cannot adequately satisfy the specified disturbance attenuation tolerance due to the presence of an under-damped complex mode in the plant transfer function. However, Thompson et al. [8] have shown that a two degree-of-freedom QFT control system could be designed to enhance the closed-loop disturbance rejection characteristics of an electrohydraulic actuator. To keep the control law as simple as possible in this paper, the actuator load pressure [1] is introduced as an internal plant state available for stability enhancing inner loop feedback. The resulting three degree-of-freedom feedback structure is shown to significantly improve the closed-loop disturbance attenuation properties of the pneumatic actuator without necessitating an increase in the complexity of the outer loop PI control law.

The three degree-of-freedom positioning system is synthesized by combining QFT with conventional root locus analysis using an outer-inner design approach. The inner loop feedback is observed to affect mainly the high frequency response. Hence, the outer loop cascade controller is designed first via QFT to set the main properties of the feedback system, i.e. robust stability margin, tracking performance, and disturbance attenuation. The inner loop feedback gain is then easily selected from the resulting root locus to provide the best damping of the troublesome closed-loop complex poles. Following this approach helps prevent the synthesis of an unnecessarily complex outer loop controller by avoiding the arbitrary selection of the inner loop feedback gain. Moreover, a satisfactory design emerges within a few iterations. Such a design procedure for pneumatic servos with load pressure feedback, within the context of QFT, has not yet been proposed in the fluid power literature. A notable exception, however, is the work of Thompson and Shukla [9] who studied QFT design with load pressure feedback in a hydraulic positioning system using an inner-outer design procedure.

II. Mathematical Modelling

A schematic of the pneumatic servoactuator under consideration is shown in Fig. 1. Assuming adiabatic charging and discharging of the actuator chambers [1], a set of nonlinear state equations that describe the dynamic system

This work was supported by the Natural Sciences and Engineering Research Council of Canada (NSERC).

M. Karpenko and N. Sepehri are with the Department of Mechanical and Industrial Engineering, University of Manitoba, Winnipeg, Manitoba, CANADA R3T 5V6

Correspondence should be sent to N. Sepehri:
nariman@cc.umanitoba.ca

is

$$\begin{aligned}\dot{x}_p &= v_p \\ \dot{v}_p &= \frac{1}{M}\left(-bv_p + AP_1 - AP_2 - F_d\right) \\ \dot{P}_1 &= \frac{\gamma RT}{V_1}\dot{m}_1 - \frac{\alpha\gamma P_1 A}{V_1}\dot{x}_p \\ \dot{P}_2 &= -\frac{\gamma RT}{V_2}\dot{m}_2 + \frac{\alpha\gamma P_2 A}{V_2}\dot{x}_p \\ \dot{x}_v &= -\frac{1}{\tau_v}x_v + \frac{k_v}{\tau_v}u\end{aligned} \tag{1}$$

In (1), x_p denotes the position of the actuator, v_p is the actuator velocity, x_v is the displacement of the valve spool, and u is the control signal. P_1, P_2, V_1, and V_2 are the instantaneous absolute actuator chamber pressures and volumes, respectively. Parameter α is a compressibility flow correction factor, which accounts for the fact that the pressure-volume work process is neither adiabatic nor isothermal, but somewhere in between [10]. F_d signifies the disturbing force that must be rejected at the plant output.

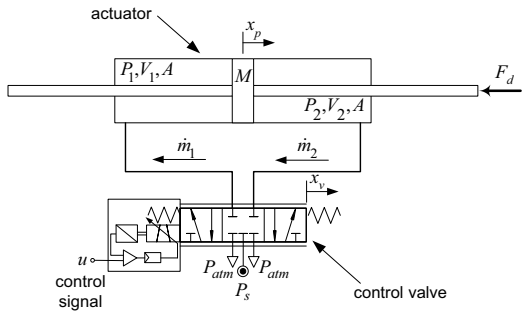

Fig. 1. Schematic of typical valve controlled pneumatic actuator.

The nonlinear equation governing the mass flow rate of air through each control valve orifice is [11]

$$\dot{m} = \begin{cases} \frac{C_1 K_f x_v P_u}{\sqrt{T}} & \text{if } \frac{P_d}{P_u} \le P_{cr} \\ \frac{C_1 K_f x_v P_u}{\sqrt{T}}\sqrt{1-\left(\frac{P_d/P_u - P_{cr}}{1-P_{cr}}\right)^2} & \text{if } \frac{P_d}{P_u} > P_{cr} \end{cases} \tag{2}$$

where $C_1 = \sqrt{\frac{\gamma}{R}\left(\frac{2}{\gamma+1}\right)^{(\gamma+1)/(\gamma-1)}}$.

In (2), P_d is the absolute downstream pressure, P_u denotes the absolute upstream pressure, and K_f is the valve gain. As suggested by Sanville [11], the critical pressure ratio, P_{cr}, which delineates between the sonic (choked) and subsonic flow regimes, is taken as 0.2.

Equation (2) may be linearized using a Taylor series expansion about operating point o. Neglecting the second and higher order terms as well as any control valve leakages, the mass flows into each actuator chamber are written as follows

$$\begin{aligned}\Delta\dot{m}_1 &= C_{f1}\Delta x_v - C_{p1}\Delta P_1 \\ \Delta\dot{m}_2 &= C_{f2}\Delta x_v + C_{p2}\Delta P_2\end{aligned} \tag{3}$$

where Δ denotes a perturbation from the operating point value, e.g. $\Delta x_v = x_v - x_{vo}$. Parameters C_{fi} and C_{pi} are known as the valve flow gain and flow-pressure coefficient, respectively. Their specific values depend upon operating point pressures, P_{1o} and P_{2o}, as well as the operating point value of valve spool displacement, x_{vo}.

Combining the Laplace transformations of equations (1) and (3) allows the operating point dependant transfer function model of the open-loop system to be written as

$$X_p(s) = G_1(s)G_2(s)U(s) - G_2(s)F_d(s) \tag{4}$$

where

$$G_1(s) = \frac{\gamma RTk_v AC_{f1}\left(\gamma RTC_{p2} + V_{2o}s\right)}{\left(\tau_v s+1\right)\left(\gamma RTC_{p1} + V_{1o}s\right)\left(\gamma RTC_{p2} + V_{2o}s\right)} + \frac{\gamma RTk_v AC_{f2}\left(\gamma RTC_{p1} + V_{1o}s\right)}{\left(\tau_v s+1\right)\left(\gamma RTC_{p1} + V_{1o}s\right)\left(\gamma RTC_{p2} + V_{2o}s\right)} \tag{5}$$

and

$$G_2(s) = \frac{\left(\gamma RTC_{p1} + V_{1o}s\right)\left(\gamma RTC_{p2} + V_{2o}s\right)}{D(s)} \tag{6}$$

with

$$D(s) = s\left(Ms+b\right)\left(\gamma RTC_{p1} + V_{1o}s\right)\left(\gamma RTC_{p2} + V_{2o}s\right) + \alpha\gamma A^2 s\left[\gamma RT\left(P_{1o}C_{p2} + P_{2o}C_{p1}\right) + \left(P_{1o}V_{2o} + P_{2o}V_{1o}\right)s\right] \tag{7}$$

Table I defines the remaining model parameters and summarizes the nominal values of all model parameters and their variations used in the controller design. The parameters and their ranges are representative of a typical low-cost industrial pneumatic servoactuator operating at 5 bars supply pressure (e.g. FESTO MPYE proportional flow control valve and a double-rod actuator with 500 mm stroke).

With respect to the characteristics of the open-loop transmission from input $U(s)$ to output $X_p(s)$, it was observed that the family of plants $\mathbf{G}(s) = \mathbf{G_1}(s)\mathbf{G_2}(s)$ are all Type 1 and minimum phase. Resonance peaking due to lightly damped complex poles of $\mathbf{G_2}(s)$ was also observed to occur around $\angle\mathbf{G} \approx -180^\circ$ thus limiting the achievable gain margin. The Bode plots of the transfer functions $\mathbf{G_2}(s)$, which relate the changes in the output $X_p(s)$ to disturbing force $F_d(s)$, also showed resonance peaking around frequency, $\omega \approx 45$ rad/sec. Consequently, it is expected that the response to step changes in the disturbing force will be oscillatory in nature.

III. QFT Controller Synthesis

Fig. 2a shows an open-loop block diagram of the pneumatic actuator, while Fig. 2b illustrates the closed-loop block diagram with dynamic pressure feedback. Transfer function $H(s)$ relating the change in the control signal, $U(s)$, to load pressure, $P_L(s) = P_1(s) - P_2(s)$, is

$$H(s) = \frac{K_{PL}\tau_{HP}s}{\tau_{HP}s+1} \tag{8}$$

In (8), parameter K_{PL} is the dynamic pressure feedback gain and τ_{HP} is the cutoff frequency of a high-pass filter.

TABLE I

LIST OF NOMINAL MODEL PARAMETERS AND THEIR RANGES.

Uncertain Parameter	Value		
	min	nominal	max
load mass, M (kg)	1.81	1.91	2.01
viscous damping coefficient, b (N·sec/m)	60	70	80
piston annulus area, A (m^3) $\times 10^{-4}$	–	10.6	–
chamber volume, V_{1o} (m^3 $\times 10^{-4}$)	1.32	2.64	3.96
chamber volume, V_{2o} (m^3 $\times 10^{-4}$)	1.32	2.64	3.96
valve spool position gain, k_v (mm/V)	–	0.25	–
valve time constant, τ_v (msec)	3.4	4.2	5.0
ideal gas constant, R (J/kg·K)	–	287	–
temperature of air source, T (K)	–	300	–
ratio of specific heats, γ	–	1.4	–
pressure-volume work correction factor, α	–	0.9	–
chamber pressure, P_{1o} (bars)	3.7	3.7	4.5
chamber pressure, P_{2o} (bars)	2.3	3.7	3.7
valve spool displacement, x_{vo} (mm)	0	0	0.125
flow gain, C_{f1} (kg/sec·m)	8.0	13.6	13.6
flow gain, C_{f2} (kg/sec·m)	8.0	13.6	13.6
flow-pressure coefficient, C_{p1} (kg/Pa·sec) $\times 10^{-10}$	0	0	118.6
flow-pressure coefficient, C_{p2} (kg/Pa·sec) $\times 10^{-10}$	0	0	51.8

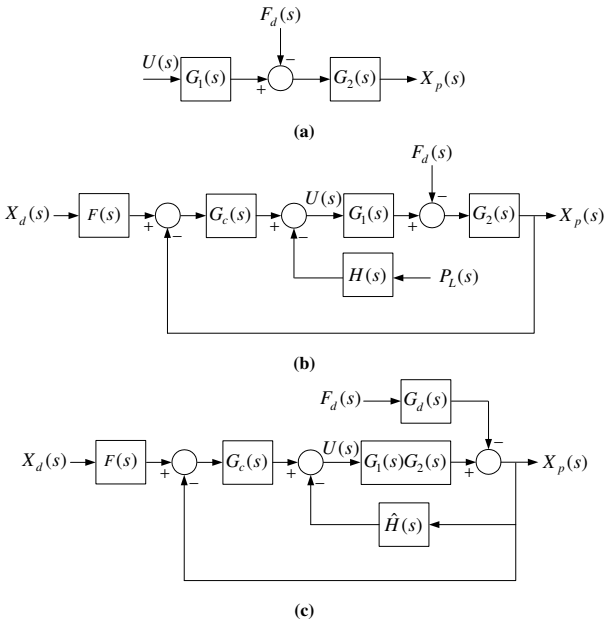

Fig. 2. Block diagram of pneumatic actuator: (a) open-loop; (b) closed-loop with dynamic pressure feedback; (c) three degree-of-freedom QFT structure.

High-pass filtering of the load pressure signal is required to ensure zero steady-state load sensitivity. When $H(s) = 0$, the pressure feedback loop is open and a two degree-of-freedom feedback structure is formed.

A three degree-of-freedom feedback control structure compatible with the QFT design methodology is shown in Fig. 2c. With reference to Fig. 2c, the closed-loop system contains two feedback loops, which may be referred to as outer and inner loops. The outer loop has transmission $L_O(s) = G_c(s)G_1(s)G_2(s)$ where subscript O denotes the outer loop. The transmission of the inner loop referred to by subscript I is $L_I(s) = G_1(s)G_2(s)\hat{H}(s)$. The transfer functions, $G_d(s)$ and $\hat{H}(s)$, required for the QFT design are

$$\hat{H}(s) = H(s)\left[Ms^2 + bs\right]A^{-1} \tag{9}$$

$$G_d(s) = G_2(s)\left[G_1(s)H(s)A^{-1} + 1\right] \tag{10}$$

For a design utilizing series compensation only, $H(s) = 0$ giving $\hat{H}(s) = 0$ and $G_d(s) = G_2(s)$.

Two important transfer functions that give the performance of the closed-loop system are now defined. The transfer function from reference input $X_d(s)$ to output $X_p(s)$ is $T(s) = \frac{X_p(s)}{X_d(s)} = F(s)\frac{L_O(s)}{1+L_I(s)+L_O(s)}$. The transfer function relating the effect of disturbing force $F_d(s)$ to changes in the output $X_p(s)$ is $T_D(s) = \frac{X_p(s)}{F_d(s)} = \frac{G_d(s)}{1+L_I(s)+L_O(s)}$. Due to the parametric uncertainty in functions $G_1(s)$ and $G_2(s)$, there exist families of closed-loop responses, denoted by $\mathbf{T}(s)$ and $\mathbf{T_D}(s)$.

The objective of the control design problem is to synthesize free elements, $F(s)$, $G_c(s)$ and $H(s)$, so that position responses, $\mathbf{x_p}(t) = \mathscr{L}^{-1}\{X_d(s)\mathbf{T}(s)\}$, and $\mathbf{x_p^d}(t) = \mathscr{L}^{-1}\{F_d(s)\mathbf{T_D}(s)\}$, fall within the prescribed time-domain tolerances. In QFT, these constraints on the closed-loop performance are used to form QFT bounds, $B(\omega)$, at a number of design frequencies, ω, with respect to nominal plant, $G_{nom}(s) = G_{1,nom}(s)G_{2,nom}(s)$. Nominal loop transmissions $L_{O,nom}(s) = G_c(s)G_{nom}(s)$ and $L_{I,nom}(s) = G_{nom}(s)\hat{H}(s)$ are then shaped by controllers $G_c(s)$ and $\hat{H}(s)$ to satisfy the QFT bounds. A more detailed discussion of QFT can be found in [7].

The closed-loop performance specifications used in the subsequent QFT controller design are given in the frequency-domain as [12]:

(i) robust stability margin

$$\left|\frac{L_O(s)}{1 + L_O(s) + L_I(s)}\right| \leq 1.24 \tag{11}$$

Equation (11) ensures minimum gain and phase margins of 5.14 dB and 45°, respectively for all plants in the set $\mathbf{G}(s)$.

(ii) tracking performance

$$|T_L(s)| \leq \left|F(s)\frac{L_O(s)}{1 + L_O(s) + L_I(s)}\right| \leq |T_U(s)| \tag{12}$$

where

$$\begin{aligned} T_L(s) &= \frac{22500}{(s+5.7)(s+10)^2(s+39.3)} \\ T_U(s) &= \frac{11.8(s+2)(s+20)}{(s+2.1)(s+15)^2} \end{aligned} \tag{13}$$

Tracking bound $T_L(s)$ gives an over-damped response with a 90% rise-time of 0.7 sec, while $T_U(s)$ has a 90% rise time of 0.2 sec and 2 percent overshoot. The bounds were derived from the relevant figures of merit for the step response of a model second-order system.

(iii) disturbance attenuation

$$\left|\frac{G_d(s)}{1+L_O(s)+L_I(s)}\right| \le \left|\frac{0.91s}{(s+5)(s^2+31.5s+2025)}\right| \quad (14)$$

Satisfaction of specification (14) ensures zero steady position error for any disturbing force, $F_d(s)$, and requires that the error due to the disturbance should be reduced to less than 2% of the peak value for $t > 0.8$ sec.

A. Design of PI Controller

A PI control law, for which $\hat{H}(s) = 0$ in Fig. 2c, was first designed to establish a closed-loop performance benchmark to which the closed-loop system with dynamic pressure feedback could be later compared. The PI control law was selected to shape $L_{O,nom}(s)$ to satisfy the QFT bounds due to its widespread use in industry. Fig. 3 shows the important QFT bounds and the designed nominal loop transmission. The PI control law, solved as ratio $\frac{L_{O,nom}(s)}{G_{nom}(s)}$, has transfer function

$$G_c(s) = \frac{K_p(s+\frac{K_i}{K_p})}{s} = \frac{15.3(s+1.7)}{s} \quad (15)$$

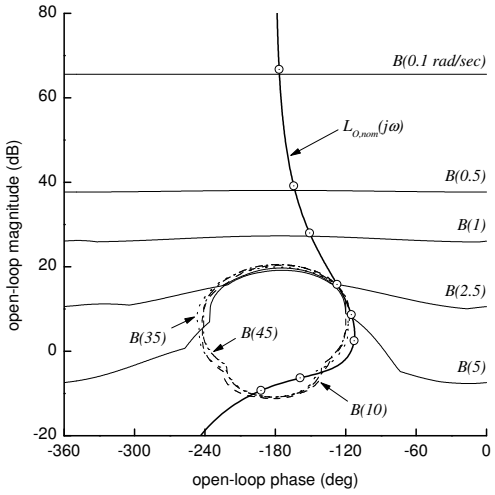

Fig. 3. QFT bounds, $B(\omega)$, and nominal outer loop transmission $L_{O,nom}(j\omega)$ without dynamic pressure feedback.

With reference to Fig. 3, $L_{O,nom}(s)$ is observed to penetrate the high-frequency bounds $B(35)$ and $B(45)$. As will be seen in Section IV, this leads to significant oscillation in the closed-loop disturbance responses. Using only a PI control law, it was impossible to increase the gain margin and place $L_{O,nom}(s)$ outside of $B(35)$ and $B(45)$ without violating the other QFT bounds. Hence, satisfaction of the bounds can only be achieved by a more complex $G_c(s)$. Prefilter $F(s)$ was synthesized via straight-line Bode approximations and has transfer function

$$F(s) = \frac{8.6(s+5.8)}{(s+2.5)(s+20)} \quad (16)$$

B. Design of PI Controller with Dynamic Pressure Feedback

To avoid the design of an unnecessarily complex outer loop controller, the outer loop was closed first and $G_c(s)$ derived to set the main properties of the feedback system. Then, the pressure feedback was designed to improve the closed-loop performance. To accommodate the inner loop closure, however, $L_{O,nom}(s)$ had to be shaped with some extra allowances at important frequencies.

With respect to outer loop transmission $L_O(s)$, the addition of the inner loop feedback was observed to give a larger gain margin, smaller phase margin, and have little effect on the plant in the low frequency range. The outer loop transmission was therefore initially designed to have a slightly larger phase margin to accommodate the subsequent inner loop closure. This was accomplished by moving the location of the zero in the PI controller (15) from $s = -1.7$ to $s = -1.5$ and adjusting the gain from 15.3 to 17.3.

Design of the feedback gains on the Nichols chart is cumbersome since $\hat{H}(s)$ appears in the feedback path. However, the required feedback gains can be easily designed using the root locus. Referring to Table I, it is observed that for the nominal plant, $V_{1o} = V_{2o} = \bar{V}$, $C_{f1} = C_{f2} = C_f$, $C_{p1} = C_{p2} = 0$, and $P_{1o} = P_{2o} = P_q$. Since the dynamics of the control valve spool are much faster than the required response of the servoactuator, the relationship between control signal and valve spool position can also be approximated as $x_v \approx k_v u$. Hence, the nominal outer loop transmission with dynamic pressure feedback is

$$L_{O,nom}(s) = \frac{2\gamma k_v C_f RTA(K_i + K_p s)}{s(Ms^2+bs)\left\{\begin{array}{c}[\bar{V}s + 2\gamma k_v C_f RTH(s)] \\ +2\gamma\alpha P_q A^2 s^2\end{array}\right\}} \quad (17)$$

The characteristic equation of (17) may be rearranged as follows to investigate the effect of pressure feedback gain, K_{PL}, on the location of the closed-loop poles

$$1 + \frac{2\gamma k_v C_f RT(Ms^2+bs^3)\tau_{HP}K_{PL}}{(\tau_{HP}s+1)\left\{\begin{array}{c}\bar{V}s(Ms^3+bs^2)+2\gamma\alpha P_q A^2 s^2 \\ +2\gamma k_v C_f RTA(K_i+K_p s)\end{array}\right\}} = 0 \quad (18)$$

The root loci of (18), with the nominal plant parameters of Table I and designed PI gains $K_p = 17.3$ V/m and $K_i = 26$ V/m·sec, are shown in Fig. 4. The cut off frequency of the high pass filter was set to 15 rad/sec.

Fig. 4 shows that two sets of complex poles are possible when the dynamic pressure feedback loop is closed. Thus, an appropriate value of feedback gain K_{PL} must balance the effects of both oscillatory modes and some iteration in the design is expected. Pressure feedback gain, K_{PL}, was first selected from the root locus to be 1.1×10^{-5} V/Pa so that both complex pole pairs were equally damped with

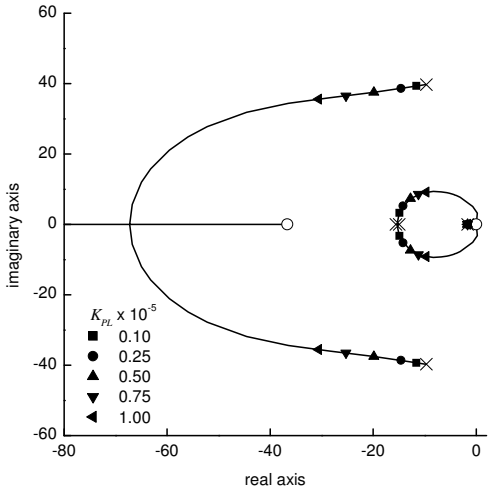

Fig. 4. Root locus of (18) for selection of pressure feedback gain, K_{PL}: ○ open-loop zeros; × open-loop poles.

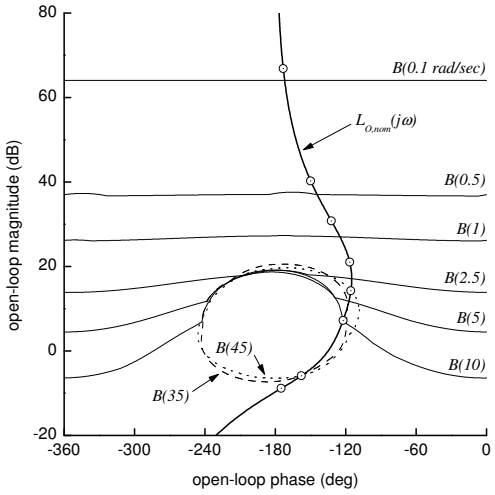

Fig. 5. QFT bounds, $B(\omega)$, and nominal outer loop transmission $L_{O,nom}(j\omega)$ with dynamic pressure feedback: design iteration 1.

$\zeta \approx 0.7$. Fig. 5 shows the resulting QFT bounds along with the redesigned outer loop transmission $L_{O,nom}(s)$.

Although the nominal loop satisfies all of the bounds, it is overdesigned in the low frequency range $\omega \leq 5$ rad/sec since in this frequency range $|L_{O,nom}(j\omega)| > B(\omega)$. An optimal design, in terms of controller gain, requires $|L_{O,nom}(j\omega)| = B(\omega)$ [13]. Hence, it is evident that a more economical solution with a lower controller gain may be obtained through some redesign.

To improve the design, either $G_c(s)$ must be made more complex to reduce the phase angle in the frequency range $\omega \leq 5$ rad/sec or the pressure feedback gain may be reduced (increasing the pressure feedback gain further complicates the design of $G_c(s)$ by reducing the phase margin). The latter option will be taken in order to keep the simple outer loop PI control law. Thus, after the design first iteration, it is apparent that $K_{PL} \leq 1.1 \times 10^{-5}$ V/Pa for a practical design. This important fact may not be immediately obvious if the inner loop is arbitrarily closed first.

Selecting $K_{PL} = 0.5 \times 10^{-5}$ V/Pa sets the damping ratio of the far-off complex pole pair at 0.47 and the damping ratio of the dominant complex pole pair at 0.87. Fig. 6 shows the recomputed bounds for $K_{PL} = 0.5 \times 10^{-5}$ V/Pa along with the redesigned $L_{O,nom}(j\omega)$. By decreasing the pressure feedback gain, the QFT bounds could be amply met by placing the zero of the outer loop PI control law at $s = -1.3$ and adjusting the gain to 20. A 10° improvement in phase margin also results. Moreover, $|L_{O,nom}(j\omega)|$ now lies closer to the corresponding $B(\omega)$ in the frequency range $0.5 \leq \omega \leq 5$ rad/sec indicating a more efficient use of the outer loop controller gain. Prefilter (16) is suitable to complete the design.

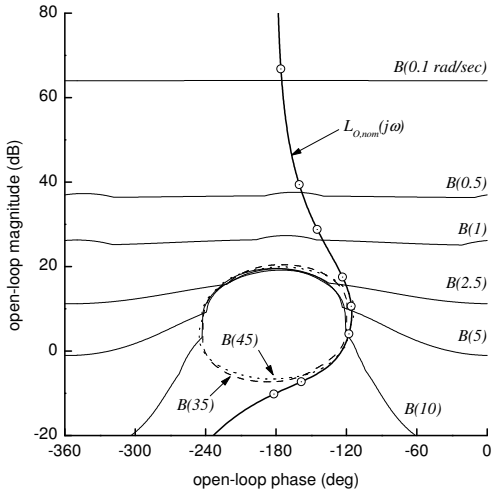

Fig. 6. Final QFT bounds, $B(\omega)$, and nominal outer loop transmission $L_{O,nom}(j\omega)$ with dynamic pressure feedback.

IV. Simulation Results and Discussion

To verify the controllers of Section III, the closed-loop frequency responses, $|\mathbf{T}(j\omega)|$ and $|\mathbf{T_D}(j\omega)|$, were obtained by computer simulations. The frequency responses $|\mathbf{T}(j\omega)|$ were within the specified tolerances. In general, the frequency responses $|\mathbf{T_D}(j\omega)|$ were also observed to meet the disturbance attenuation specification, i.e. $|\mathbf{T_D}(s)| \leq |M_D(s)|$. However, the resonance peaks in $|\mathbf{T_D}(s)|$ under PI control without pressure feedback penetrated the $M_D(s)$ bound.

Fig. 7 shows the family of closed-loop unit step responses, $\mathbf{x_p}(t) = \mathscr{L}^{-1}\{s^{-1}\mathbf{T}(s)\}$ pertaining to each of the designed control systems. As is seen, the unit step responses are nearly identical for both control systems, suggesting that implementation of the inner loop feedback does little to affect the closed-loop reference tracking performance. The similarity in the responses is mainly due to the fact that the low-pass effect of the prefilter attenuates any resonance peaking in transfer functions $\mathbf{T}(s)$. Consequently, no resonance oscillations are observed in time responses.

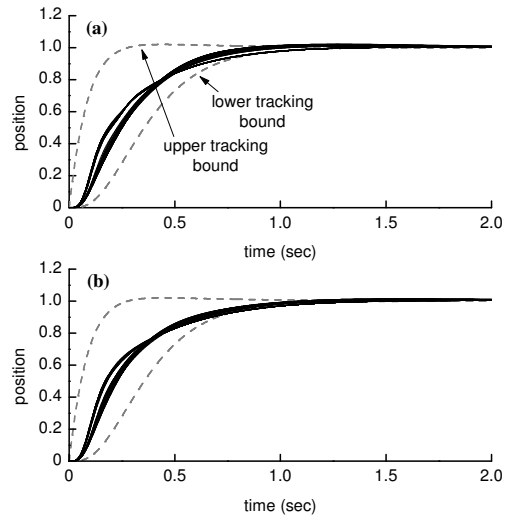

Fig. 7. Closed-loop unit step responses $\mathbf{x_p}(t)$: (a) PI control only; (b) PI control with dynamic pressure feedback.

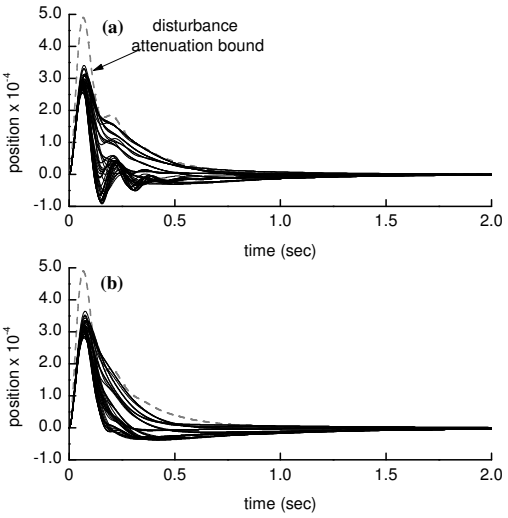

Fig. 8. Closed-loop responses to unit step disturbance $\mathbf{x_p^d}(t)$: (a) PI control only; (b) PI control with dynamic pressure feedback.

The simulated time-domain responses to unit step disturbances, $\mathbf{x_p^d}(t) = \mathscr{L}^{-1}\{s^{-1}\mathbf{T_D}(s)\}$ are shown in Fig. 8. As is seen, the inner loop feedback eliminates the oscillation and reduces the overshoot associated with the design where $\hat{H}(s) = 0$. Evidently, the inner loop feedback improves the damping of the troublesome under-damped complex plant poles thereby reducing the peaking in transfer functions $\mathbf{T_D}(s)$. Hence, from the perspective of rejection of disturbing forces, the use of inner loop pressure feedback is clearly justified.

V. Conclusions

The QFT design of a simple PI position controller for a typical industrial pneumatic actuator having internal load pressure feedback has been addressed for the first time. It was observed that a PI control law alone could not adequately satisfy the disturbance attenuation specification due to resonance peaking caused by under-damped closed-loop complex poles. However, measurement of the load pressure provided an internal state variable that was exploited for stability enhancing inner loop feedback. The inner loop closure was observed to significantly improve the closed-loop disturbance responses without increasing the complexity of the outer loop control law. The use of dynamic pressure feedback for improvement of the closed-loop disturbance attenuation characteristics of pneumatic servos is thus justified.

References

[1] S. Liu and J.E. Bobrow, "An Analysis of a Pneumatic Servo System and its Application to a Computer-Controlled Robot," *ASME Journal of Dynamic Systems, Measurement and Control*, vol. 110, no. 3, pp. 228-235, 1988.

[2] A.K. Paul, J.K. Mishra, and M.G. Radke, "Reduced Order Sliding Mode Control for Pneumatic Actuator," *IEEE Transactions on Control Systems Technology*, vol. 2, no. 3, pp. 271-276, 1994.

[3] D.C. Gross and K.S. Rattan, "A Feedforward MNN Controller for Pneumatic Cylinder Trajectory Tracking Control," *International Conference on Neural Networks*, Houston, TX, vol. 2, pp. 794-799, 1997.

[4] S. Chillari, S. Guccione, and G. Muscato, "An Experimental Comparison Between Several Pneumatic Position Control Methods," *40th IEEE Conference on Decision and Control*, Orlando, FL, pp. 1168-1173, 2001.

[5] Q. Yang, Z. Wang, and J. Lu, "Pneumatic Servo System Control via Nonlinear H_∞ Control and Direct Feedback Linearization," *Journal of Nanjing University of Science and Technology*, vol. 26, no. 1, pp. 52-56, 2002.

[6] F. Xiang and J. Wikander, "QFT Control Design for an Approximately Linearized Pneumatic Positioning System," *International Journal of Robust and Nonlinear Control*, vol. 13, no. 7, pp. 675-688, 2003.

[7] I.M. Horowitz, *Quantitative Feedback Design Theory - QFT*, vol. 1. Boulder, CO: QFT Publications, 1993.

[8] D.F. Thompson, J.S. Pruyn, and A. Shukla, "Feedback Design for Robust Tracking and Robust Stiffness in Flight Control Actuators Using a Modified QFT Technique," *International Journal of Control*, vol. 72, no. 16, pp. 1480-1497, 1999.

[9] D.F. Thompson and A. Shukla, "Robustness Aspects of Pressure Differential Feedback in Hydraulic Servomechanisms: A QFT Approach," *Proceedings of the Institution of Mechanical Engineers: Part I, Journal of Systems and Control Engineering*, in review, 1999.

[10] E. Richer and Y. Hurmuzlu, "A High Performance Pneumatic Force Actuator System: Part I - Nonlinear Mathematical Model," *ASME Journal of Dynamic Systems, Measurement and Control*, vol. 122, no. 3, pp. 416-425, 2000.

[11] F.E. Sanville, "A New Method of Specifying the Flow Capacity of Pneumatic Fluid Power Valves," *BHRA 2nd International Fluid Power Symposium*, Guildford, England, pp. D3-37-D3-47, 1971.

[12] M. Karpenko and N. Sepehri, "Robust Position Control of an Electrohydraulic Actuator with a Faulty Actuator Piston Seal," *ASME Journal of Dynamic Systems, Measurement and Control*, vol. 125, no. 3, pp. 413-423, 2003.

[13] A. Gera and I. Horowitz, "Optimization of the Loop Transfer Function," *International Journal of Control*, vol. 31, no. 2, pp. 389-398, 1980.